

## Determination of Ochratoxin at Nanocomposite Modified Glassy Carbon Electrode Combine with FFT Coulometric Admittance Voltammetry and Flow Injection Analysis

Parviz Norouzi<sup>1,2,\*</sup>, Iraj Alahdadi<sup>3,\*</sup>, Seyed Jamaledin Shahtaheri<sup>4</sup>

<sup>1</sup> Center of Excellence in Electrochemistry, Faculty of Chemistry, University of Tehran, Tehran, Iran

<sup>2</sup> Biosensor Research Center, Endocrinology & Metabolism Molecular-Cellular Sciences Institute, Tehran University of Medical Sciences, Tehran, Iran

<sup>3</sup> Department of Agronomy and Plant Breeding, College of Abouraihan, University of Tehran, Tehran, Iran

<sup>4</sup> Departments of Occupational Health, School of Public Health, and Institute for Environmental Research, Tehran University of Medical Sciences, Tehran, Iran

\*E-mail: [norouzi@khayam.ut.ac.ir](mailto:norouzi@khayam.ut.ac.ir)

Received: 20 December 2014 / Accepted: 9 February 2015 / Published: 24 February 2015

---

In this work, a new electrochemical technique based on combination of FFT Coulometric Admittance Voltammetry (FFTCAV) technique and a nanocomposite electrode was developed for the determination of Ochratoxin A in a flow- injection system. The sensor was designed by deposition of gold nanoparticles on reduced graphene nanosheets mixed with carbon multiwall nanotube and ionic liquid (1-ethyl-3-methyl-imidazolium ethylsulphate) casted on a glassy carbon electrode. Also, in this technique the sensor response calculated in form of charge changes under the peak by integrating admittance in selected potential range, after subtracting the background admittance. As results, application of the nanocomposite as a modifier can catalyze electron transfer, which causes amplifying the response. Besides, it was found the electrode response was proportional to concentrations of Ochratoxin A in range from 0.1 to 200 nM, with a detection limit of  $3.7 \times 10^{-12}$  M. The nanocomposite electrode showed good reproducibility, a long-term of usage stability for 90 days. The characterization of the sensor surface was studied by scanning electron microscopy and electrochemical impedance spectroscopy methods.

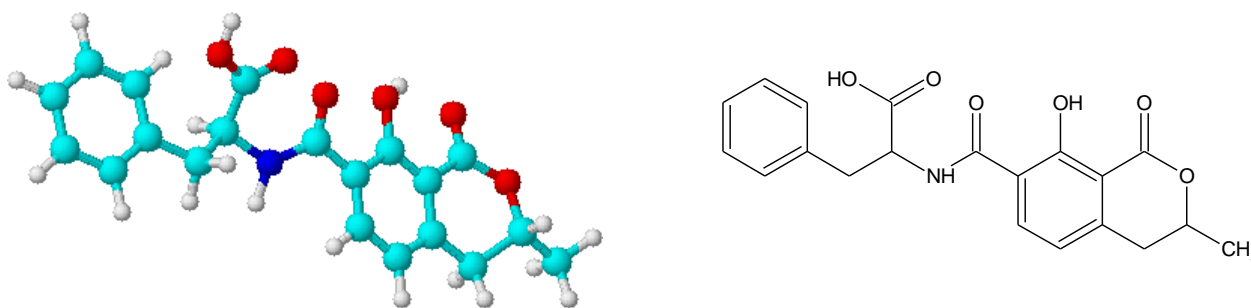
---

**Keywords:** nanocomposite, FFT Coulometric Admittance Voltammetry, Ochratoxin A, ionic liquid

### 1. INTRODUCTION

By industrialization of human life, many organic species come in to the environment and affect human health [1-5]. Many toxic compounds enter the ground water in agricultural lands [6,7].

Ochratoxin A (OCA) is one of the organic compounds widely used throughout the world in agricultural applications, especially used as a contaminant of improperly stored food products, particularly in northern climates of Europe and North America. The chemical structure of OCA is shown in Scheme 1. Because, OCA is a toxin produced by *Aspergillus ochraceus*, *Aspergillus carbonarius* and *Penicillium verrucosum*, is one of the most plentiful food-contaminating mycotoxins. It is quite efficient against broad leaved and grassy weeds in crops including corn, coriander, sugarcane, sorghum, orchard and grass [18]. Also, their derivatives can remain in soils, natural waters and other environmental domains for a long time [29,310]. Some instrumental methods are reported for the determination of OCA [11, 12]. In designing of new sensors, the unique characterization of gold nanoparticles (Au NPs) providing a suitable microenvironment for facilitating electron transfer between the organic compounds and electrode surfaces. As well, it was noted that Au NPs were used to incorporate with other nanomaterial has been found efficiently enhancing the electron transfer reactivity of the electrode surface.



**Scheme 1.** Chemical structure of Ochratoxin A

Some instrumental methods are reported for the determination of OCA[411,512]. In designing of new sensors, the unique characterization of gold nanoparticles (AuNPs) providing a suitable microenvironment for facilitating electron transfer between the organic compounds and electrode surfaces. As well, it was noted that Au NPs were used to incorporate with other nanomaterial has been found efficiently enhancing the electron transfer reactivity of the electrode surface.

It is well known that nanomaterials of carbon, like reduced graphene nanosheets (RGNS) demonstrate high surface area and excellent electrical conductivity in new designed electrodes. Moreover, it helps to establish a larger number of active sites for adsorption of organic molecules, which have led to a wide use of this nanomaterial in structure of electrochemical sensors and biosensor [613-815].

Furthermore, in order to improve the performance of the carbon paste electrode, ionic liquids (IL) can be very helpful as a binder in the carbon pate electrodes. Now, IL was used as a binder in the nanocomposite electrode to its high ionic conductivity, good stability and well biocompatibility. The excellent characterizations of RGNS and Au NPs mixture can facilitate the redox reaction of electroactive species [916, 1017].

Fast Fourier transformation (FFT) Voltammetric voltammetric techniques are widely used in determination of various organic compounds [1118-1725]. In this work, the main objective is the first application of FFT Coulometric Admittance Voltammetry (FFTCV) technique was used to investigate the electrochemical response of OCA on the surface of the nanocomposite glassy carbon electrode. The presence of Au NPs and RGNS in modification of the electrode provides an environment, which could improve the sensitivity of the measurement. Scanning electron microscopy (SEM) and impedance spectroscopy (EIS) was used to characterize the sensor surface. Under the optimal conditions, the proposed modified electrode exhibited a linear response to a wide concentration range of OCA.

## 2. MATERIALS AND METHODS

### 2.1. Reagents

All chemicals and solvents used were of analytical grade and were used as received. 1-ethyl-3-methyl-imidazolium ethylsulphate (IL), was purchased from Aladdin-Reagent Company (China). Ochratoxin A and  $\text{HAuCl}_4$  were purchased from Sigma–Aldrich. Graphene nanosheets purchased from Sinopharm Henan Bonzer Imp. Gold nanoparticles were produced by reducing  $\text{HAuCl}_4$  on electrode surface. The mean size of the prepared Au colloids was about 25 nm, estimated by transmission electron microscopy in a separate experiment. The solution 3 mM  $\text{Fe}(\text{CN})_6^{4-/3-}$  in 0.1 M KCl. Double distilled water was used throughout the experiment.

### 2.3. The sensor fabrication

The schematic step of the sensor preparation is steps of the sensor preparation are shown in Figure 1. A glassy carbon electrode, (GCE, 3 mm in diameter) was polished, well, with 1.0, 0.3 and 0.05  $\mu\text{m}$  alumina slurry and then it was washed thoroughly with doubly distilled water. The electrodes were successively sonicated in 1:1 nitric acid, acetone and doubly distilled water, and then allowed to dry at room temperature. Primarily, Graphene nanosheets Oxide (GNSO) was prepared by a modified Hummers method using expandable graphite flake as the original material [1826]. 1g expandable graphite flake was mixed with 45 g NaCl for 15 min, and subsequently NaCl was dissolved in water and removed by filtration.

The RGSN was prepared by a chemical reduction of the 0.6 mg/ml GNSO powder in distilled water with 160 mM  $\text{NaBH}_4$  [1927]. The mixture was heated (90 °C) for 35 min. The product was centrifuged to precipitate the RGNS powder, which was eventually dried in vacuum at low temperature. Meanwhile, the MWCNTs-COOH was synthesized by chemically treating with strong carboxyl acid for purification and surface modification. A 1.2 g sample of MWCNTs was heated to reflux (110 °C) in a 3:1  $\text{H}_2\text{SO}_4:\text{HNO}_3$  solution for 30 min. After washing the treated sample, the black product was dried at 80 °C under vacuum. Subsequently, 10 ml homogeneous RGNS dispersed in aqueous solution was mixed with IL and MWCNTs-COOH and stirred for 30 min to form a

homogeneous aqueous solution. And then, 50  $\mu\text{L}$  of the composite materials was dropped on the cleaned GCE and dried naturally to construct the modified electrode. The electrode was rinsed throughout with doubly distilled water. For obtaining Au NPs/RGNS-MWCNT-IL/GCE, the electrochemical deposition of Au NPs was performed in 0.2 M  $\text{Na}_2\text{SO}_4$  aqueous solution of  $\text{HAuCl}_4$  (1.0 mM) (the potential was -0.2 V).

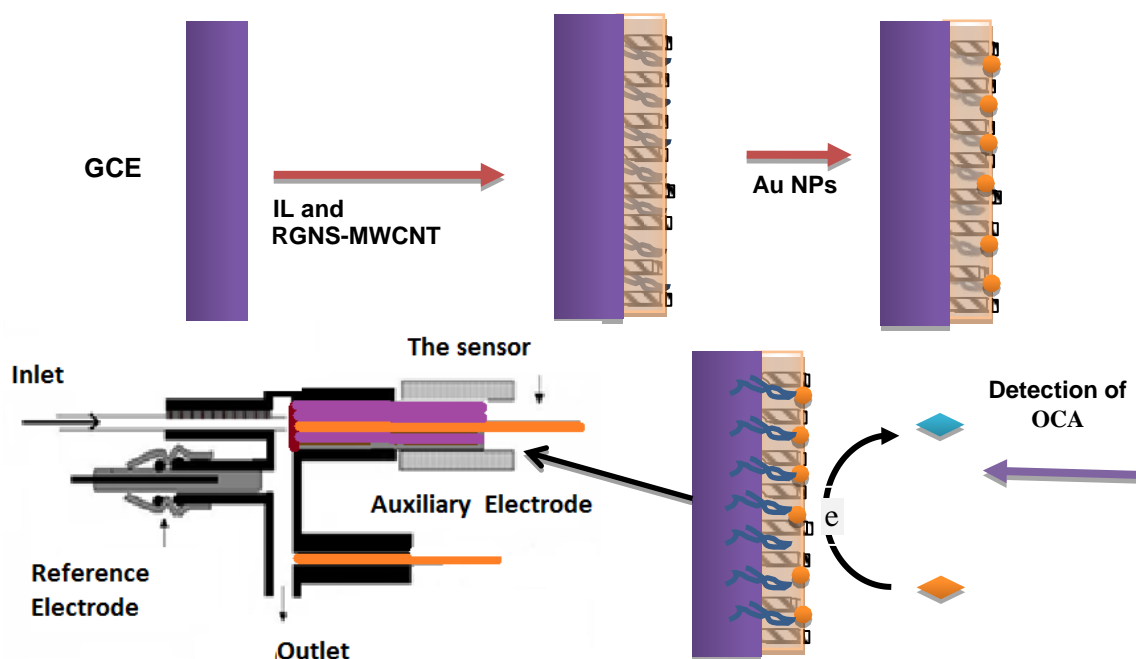


**Figure 1.** , Schematic steps of the sensor preparation, b) the electrochemical cell used in flow injection analysis

### 2.3. Flow injection system

The flow injection analysis use for measurements, the equipment was integrated with an eight roller peristaltic pump (Ultratech Labs Co., Iran) and a five way injection valve (Ultratech Labs Co., Iran, Fig. 2 inset) with 600  $\mu\text{L}$  sample injection loop. The electrochemical FFTCAV was carried out with a homemade potentiostat was connected to a PC equipped with an analog to digital data acquisition board (PCL-818H, Advantech Co.). Electrochemical cell was a conventional three-electrode system with a working electrode, a platinum wire as an auxiliary electrode and a saturated calomel electrode (SCE) as reference electrode. The condition for the data acquisition requirements electrochemical software was developed using Delphi 6.0. The program was used to generate an analog waveform and acquire current readings. The modified potential waveform is shown in Fig. 2D, which was continuously applied to the working electrode. Then data was acquired, and stored by the software. Also, the software was able to process and plot the data in real time. EIS measurements were

performed in 3 mM  $K_3Fe(CN)_6$  in 0.1 M KCl. A stock solution of 2mM of OCA was firstly prepared, and then an aliquot was diluted to the appropriate concentration.

### 3. RESULTS AND DISCUSSION

The response of sensor is related to its morphology. Therefore, the surface of sensor was examined by SEM technique. Fig. 2A and B present the typical SEM images of the GCE and AuNPs/RGNS-MWCNT-IL/GCE surface, respectively. In Fig. 2A, it could be seen that RGNS showed the typical crumpled structure, and the magnitude and scattering of Au NPs on the surface. Correspondingly, in some sections, the SEM image of Au NPs/RGNS-MWCNT-IL/GCE exhibits granular morphology with average grain size of about 100–150 nm. It seems that the

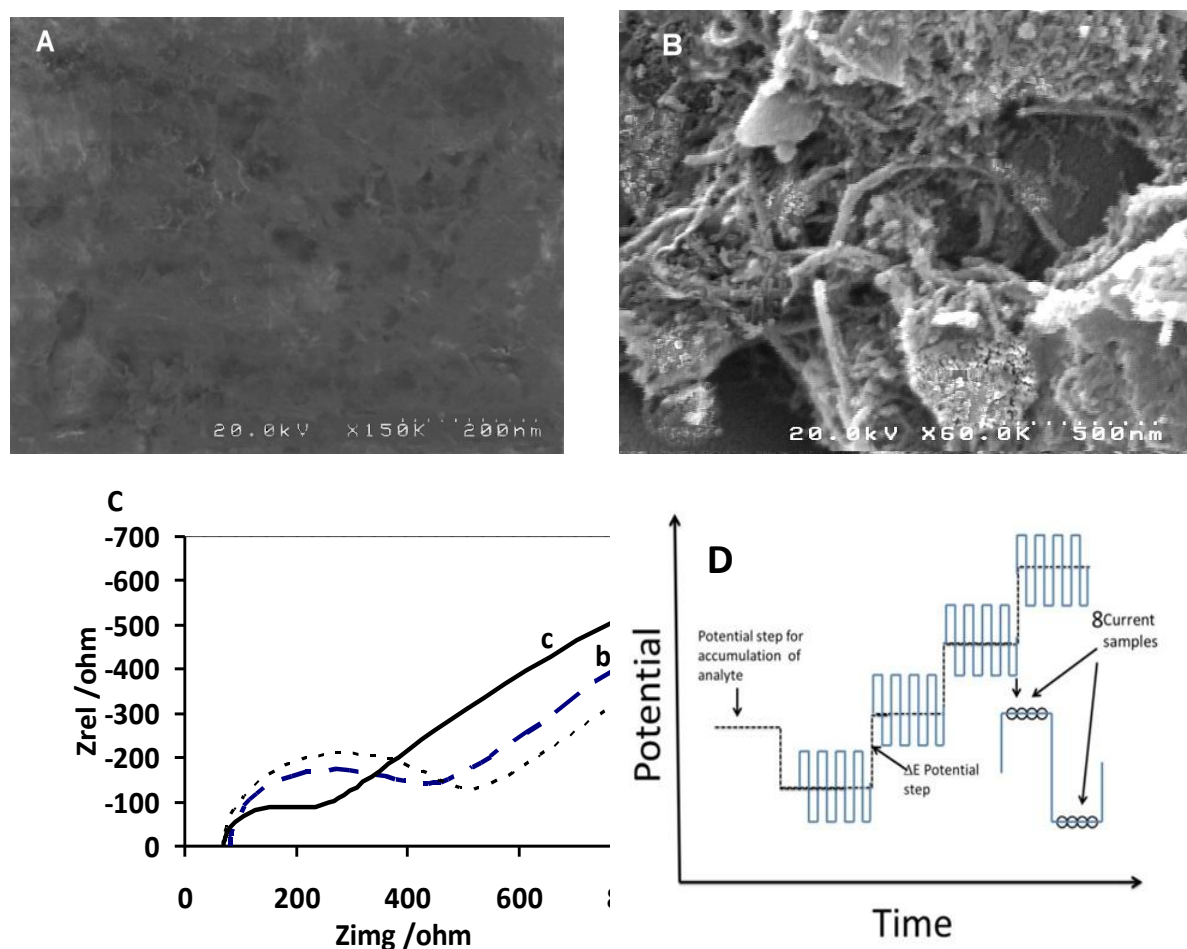


**Figure 2.** SEM image of A)GCE, B) AuNPs/RGNS-MWCNT-IL/GCE sensor, C) EIS plots of modified electrode in 3 mM  $K_3Fe(CN)_6$  with 0.1 M KCl: (a) bare GCE (b) RGNS-MWCNT-IL/GCE and (c) AuNPs/RGNS-MWCNT-IL/GCE .D), The diagram of the FFTCAV potential waveform.

Formation of RGNS-IL layer on the surface of GCE is necessary to reach a sufficient thickness to create a satirically a good porosity and stabilized Au NPs on the surface. In fact, the composite surface is well-coated with AuNPsRGNS the diameters 20–90 nm. Moreover, the surface of the electrode was predominated by isolated and regularly shaped RGNS and MWCNT particles. The fragments of Au NPs dispersion was stabilized by IL and RGNS.

Fig. 2C demonstrates EIS curves for the unmodified GCE, RGNS-MWCNT-IL/GCE and AuNPs/RGNS-MWCNT-IL/GCE in 0.1 M KCl solution containing 3 mM  $[\text{Fe}(\text{CN})_6]^{3-/4-}$ , respectively. The results suggested that the  $R_{ct}$  (charge transfer impedance) of RGNS-MWCNT-IL/GCE (curve b) was lower than that was obtained for the bare GCE electrode (curve a). This could be of a higher collection of  $[\text{Fe}(\text{CN})_6]^{3-/4-}$  species on the sensor surface due to the existing a large area. Likewise, the change the value of  $Z_{rel}$  for AuNPs/RGNS-MWCNT-IL/GCE sensor shown in curve c, the value of  $R_{ct}$  decreased, which indicates that Au NPs and RGNS-MWCNT-IL encompass an excellent electrical conductive materials, which can enhance the electron transfer of  $[\text{Fe}(\text{CN})_6]^{3-/4-}$  at the electrode surface.

Fig. 2C demonstrates EIS curves for the unmodified GCE, RGNS-MWCNT-IL/GCE and AuNPs/RGNS-MWCNT-IL/GCE in 0.1 M KCl solution containing 3 mM  $[\text{Fe}(\text{CN})_6]^{3-/4-}$ , respectively. The results suggested that the  $R_{ct}$  (charge transfer impedance) of RGNS-MWCNT-IL/GCE (curve b) was lower than that was obtained for the bare GCE electrode (curve a). This could be of a higher collection of  $[\text{Fe}(\text{CN})_6]^{3-/4-}$  species on the sensor surface due to the existing a large area. Likewise, the change the value of  $Z_{rel}$  for AuNPs/RGNS-MWCNT-IL/GCE sensor shown in curve c, the value of  $R_{ct}$  decreased, which indicates that AuNPs and RGNS-MWCNT-IL encompass excellent electrical conducting materials, which can enhance the electron transfer of  $[\text{Fe}(\text{CN})_6]^{3-/4-}$  at the electrode surface.

### 3.1. Analytical procedure for determination of OCA

Fig. 2D shows the potential waveform used for FFTCAV measurements, which was continuously applied to the working electrode during an experimental runa measurement. As shown in the figure, the measurement part of the waveform contains multiple SW square wave (SW) polarization cycle with amplitude of  $E_{sw}$  and frequency  $f_o$ , were superimposed on a staircase potential, which was changed by a small potential step of  $\Delta E$  (10 mV). The value of  $E_{sw}$  could be in the range of 5-100 mV. In a potential ramp, the currents were sampled eight times per each SW polarization cycle. It This is advantageous in FFTCAV to collect more current samples in forward and reverse SW pulses and use signal averaging to increase the S/N. . Finally, FFTCAV technique could able to sample the current across the entire a SW period and use for calculating the admittance of the electrode. Fig.3 shows the three dimensional net admittance changes in the voltammograms in the potential range of -200 to 950 mV. The time axis represents the time passing of the experiment and the sweep number. The figure shows that at the beginning of the experiment there is no signal insignal in the the subtracted voltammograms, but after addition of  $12.0 \times 10^{-7}$  M OCA in 0.05 M BPS, where a peak

appears at potential 500 mV. The increase in the admittance at this potential is due to the electrochemical reaction of OCA at AuNPs/RGNS-MWCNT-IL/GCE surface.

In this detection technique, the sensor response was calculated based on the charge under peak in the recorded admittances [2028-2634]. The unit for the resulted signal is change from ampere to coulomb (C), which is the charge changes ( $\Delta Q$ ) under the voltammograms curve at a selected potential range,  $E_1$  to  $E_2$ . The equation for the response is calculated as follows,

$$\Delta Q_n = Q_n - Q_{ave} \quad \text{for } n > 0 \tag{1}$$

or

$$\Delta Q_n = \Delta t \left[ \int_{E_1}^{E_2} A(s, E) \cdot E \cdot dE + ave \int_{E_1}^{E_2} A(s, E) \cdot E \cdot dE \right] \tag{2}$$

$$\Delta Q (s \tau) = \Delta t \left[ \sum_{E=E_1}^{E=E_2} A(s, E) \cdot E - \sum_{E=E}^{E=E_2} A(s_r, E) \cdot E \right] \tag{3}$$

where  $Q$  is the electrical charge obtained by integration of admittance voltammetric curve between 100 and 800 mV, and  $Q_0$  represents  $Q$  in the absence of the adsorbent.  $s$  is the sweep number,  $\tau$  is the time period between subsequent sweeps,  $\Delta t$  is the time difference between two subsequent points on the FFTCAV curves,  $A (s, E)$  represents the admittance of the FFTCAV curve recorded during the  $s$ -th sweep and  $A(s_r, E)$  is the reference admittance of the FFTCAV curve.

$E_1$  and  $E_2$  are the initial and the vertex potential, respectively. The reference FFTCAV curve was obtained by averaging a few FFTCAV curves (3-5) recorded at the beginning of the experiment measurement, before the injection of the analyte OCA solution. By optimizing important parameters, the FFTCAV amplitude and frequency and selecting suitable flow rate of the electrochemical response, the S/N response can be increased.

### 3.2. The effect of nanocomposite content

Fig. 5 demonstrates the change of the sensor response with the amount of RGNS and Au NPs in the content of AuNPs/RGNS-MWCNT-IL composition. The injected solution was  $2.0 \times 10^{-7}$  M OCA in the buffer solution at pH 7.0, and the integration potential range, for calculating the response of the sensor, was 0 to 800 mV at frequency 400 Hz and amplitude 25 mV. Where, different amounts of RGNS (0.1 to 2.5 mg) in optimum quantity of MWCNT-IL suspension solution were casted on the electrode surface. In these measurements, also, various deposition times of Au NPs (5 to 200 s) were tested.

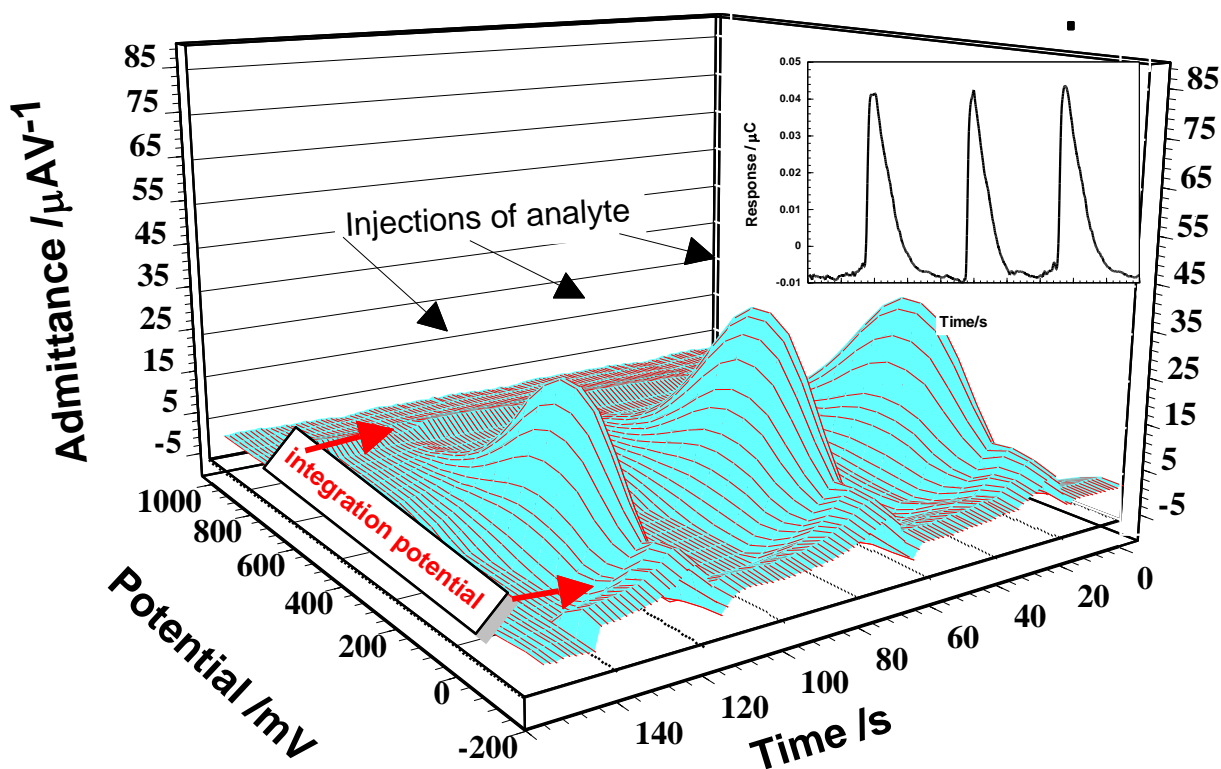


**Figure 3.** Substracted FFT admittance voltammograms of the Au NPs/RGNS-MWCNT-IL/GCE sensor in absent and with addition of  $2.0 \times 10^{-7}$  M OCA in buffer solution at pH 7.0; at frequency 400 Hz and amplitude 25 mV. The inset is sensor response by integration of admittance in potential range 0 to 800 mV.

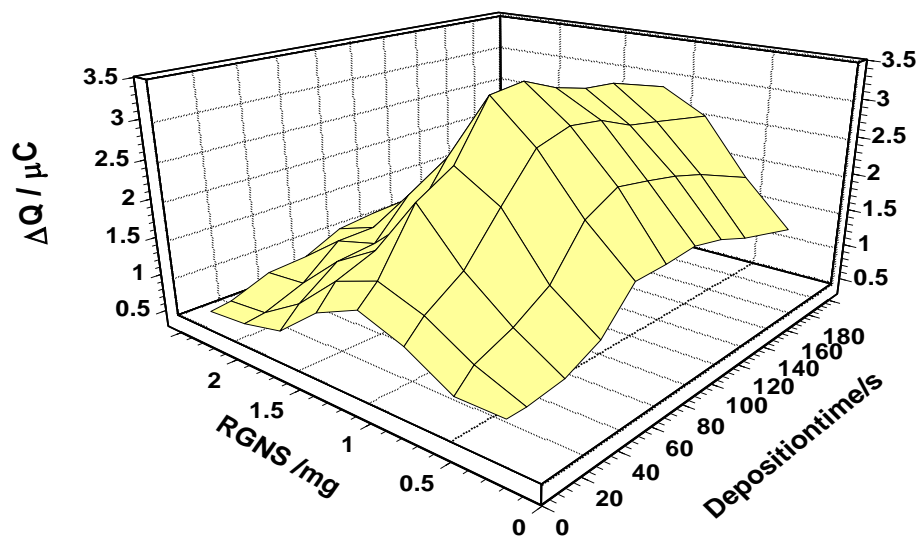


**Figure 5.** The effect of deposition time for Au NPs and RGNS on the response of Au NPs/RGNS-MWCNT-IL/GCE in  $2.0 \times 10^{-7}$  M solution of OCA at pH 7.0. In the potential range of -200 to 950 mV at frequency 400 Hz and amplitude 25 mV. Integration potential range for the admittance was 0 to 800 mV

The graph indicates that the value of  $\Delta Q$  increases with the increasing of RGNS up to 1.2 mg and then decreases. Moreover, as shown in the figure, in case of Au NPs, the value of  $\Delta Q$  increases with the deposition time for Au NPs on the sensor composition up to 120 s. Whereas, at the higher the deposition time of Au NPs,  $\Delta Q$  changes minor. This could be due to unchanged the surface area sensor at the additional deposition time Au NPs.

### 3.2. Optimization of FFTCAV frequency and amplitude

Due to this fact that the SW frequency acts similar to sweep rate in cyclic voltammetry method, consequently, the background noise, and the peak shape could rely on the speed of the excitation signal. Consequently, the admittance in FFTCAV, the SW frequency and amplitude are important factors in the value of admittance and the sensitivity of the measurements. , in FFTCAV technique. For the same reason, Consequently, the the coulometric response of Au NPs/RGNS-MWCNT-IL/GCE to OCA depends on the applied value SW frequency and amplitude. To obtain the optimum SW waveform condition in for maximum  $\Delta Q$ , the SW frequency in range 100-700 Hz and amplitude in range 5 to 50 mV were investigated studied.

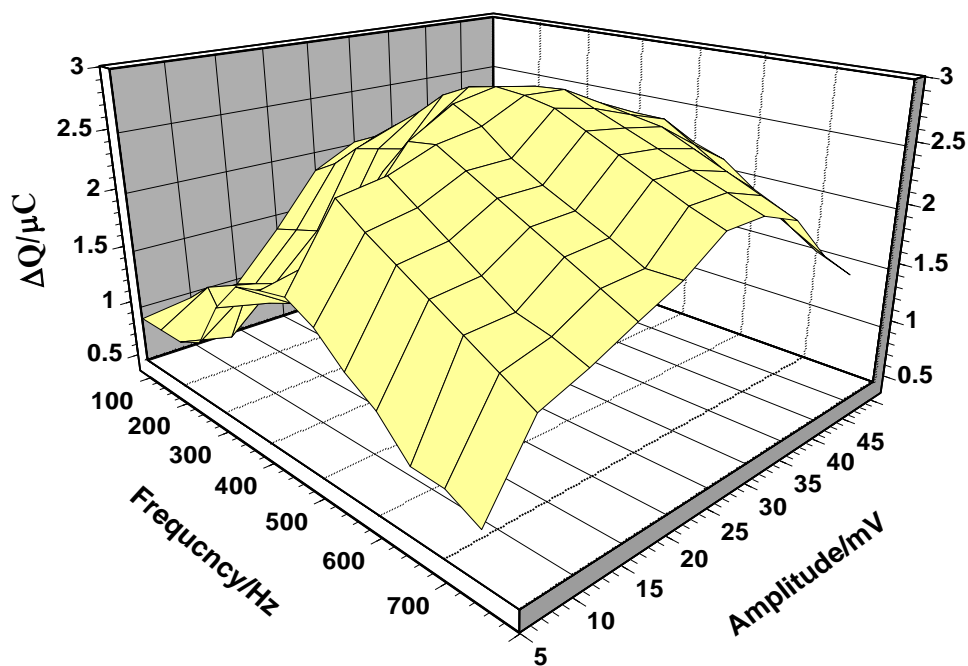


**Figure 4.** The effect of frequency and amplitude on the response of Au NPs/RGNS-MWCNT-IL/GCE to injection of  $2.0 \times 10^{-7}$  M OCA in buffer solution at pH 7.0, the potential range of -200 to 950 mV. Integration potential range for the admittance is 0 to 800 mV

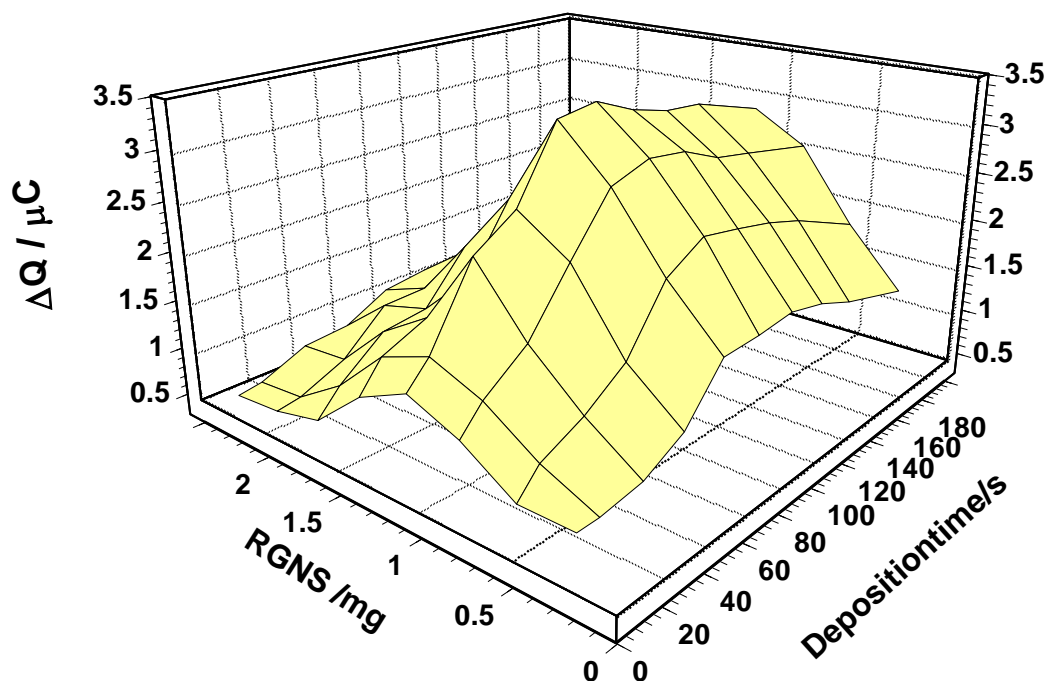
In Fig. 4 the importance of frequency and amplitude is demonstrated demonstrates of the alteration of the sensor response for in solution of  $12.0 \times 10^{-7}$  M of OCA with frequency and amplitude.

As seen in the graph, the increasing the SW frequency and amplitude will amplify increase the admittance value of the Au NPs/RGNS-MWCNT-IL/GCE, which may due to enhancement in value of the current. The figure, also, shows enhancement frequency up to 400 Hz and amplitude up to 25 mV the value of  $\Delta Q$  increase up to  $2.6 \mu\text{C}$ , and after that a decline in the response can be observed.

Nevertheless, the increasing elaboration the SW frequency will increase the SW peak current admittance, or the sensitivity of the technique, but this will be tempered by a higher charging/faradic current ratio. It should be noted that in this case, the solution resistance, electrode sensor diameter, and stray capacitance of the system will limit the sensitivity gains obtained by raising the SW frequency and amplitude. Also, it could be suggested that at the higher values of frequency and amplitude by reason of due to offered a shorter time for the electrochemical process on the sensor surface, consequently, the response becomes smaller.

Yet, In in FFTCAV technique, application SW frequencies lower than 400 Hz causes a longer potential scan times, which result to lower number of voltammetric scan (as well as the data points for the response peak) for each injected sample zone.

### 3.2. The effect of nanocomopite content



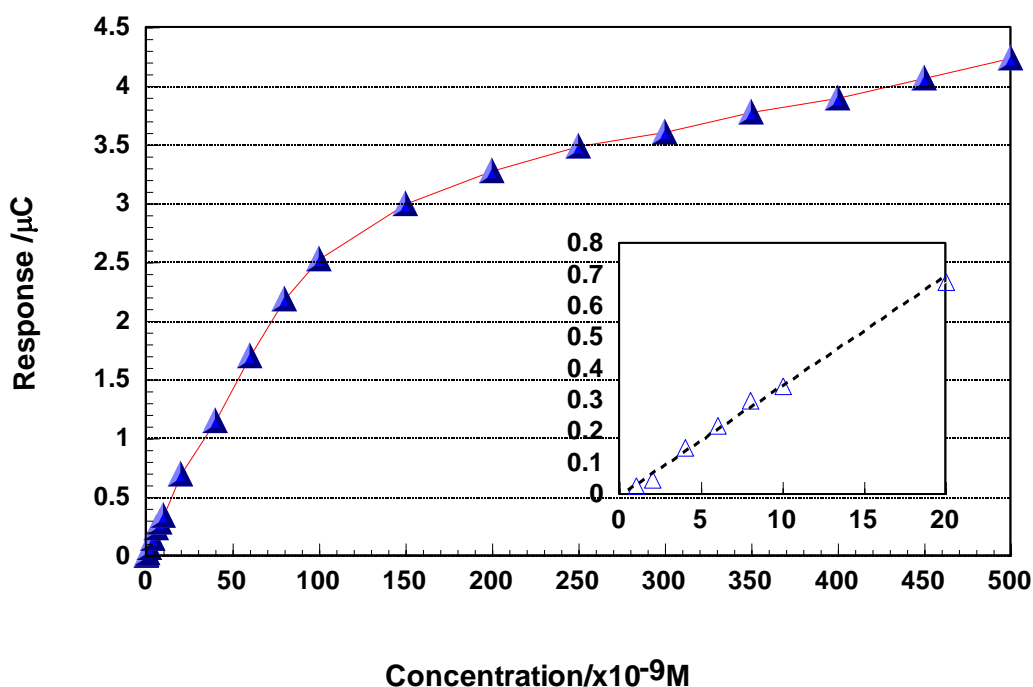
**Figure 5.** The effect of deposition time for Au NPs and RGNS on the response of Au NPs/RGNS-MWCNT-IL/GCE in  $2.0 \times 10^{-7}$  M solution of OCA at pH 7.0. In the potential range of -200 to 950 mV at frequency 400 Hz and amplitude 25 mV. Integration potential range for the admittance was 0 to 800 mV

Fig. 5 demonstrates the change of the sensor response with the amount of RGNS and Au NPs in the content of Au and RGNS in Au NPs/RGNS-MWCNT-IL/GCE composition. The injected solution was  $2.0 \times 10^{-7}$  M OCA in the buffer solution at pH 7.0, and the in-gratiation potential range, for calculating the response of the sensor, was 0 to 800 mV at frequency 400 Hz and amplitude 25 mV. Where, different amounts of RGNS (0.1 to 2.5 mg) in optimum quantity of MWCNT-IL suspension solution were casted on the electrode surface. In these measurements, also, various deposition times of Au NPs (5 to 200 s) were tested.

The graph indicates that the value of  $\Delta Q$  increases with the increasing of RGNS up to 1.2 mg and then decreases. Moreover, as shown in figure, for Au NPs the value of  $\Delta Q$  increases with the deposition time for Au NPs on the sensor composition up to 120 s. Whereas,  $\Delta Q$  almost remained constant at the higher volume of Au NPs solution. This could be due to unchanged the surface area sensor at more Au NPs.

### 3.5. Calibration curve

The electrochemical reaction of OCA on the electrode surface will increase the admittance of sensor. Fig. 6 shows that the  $\Delta Q$  response performances exhibits a dynamic correlation with the concentration of OCA with FFTCAV technique method. A linear correlation of Au NPs/RGNS-MWCNT-IL/GCE to OCA from 0.2 to 500.0 nM in buffer solution at pH 7.0 in the potential range of -200 to 9500 mV at frequency 400 Hz and amplitude 25 mV.



**Figure 6.** Response of the Au NPs/RGNS-MWCNT-IL/GCE to OCA concentrations: 0.2 to 500 nM in AB buffer solution at pH 7.0, in the potential range of -200 to 950 mV at frequency 400 Hz and amplitude 25 mV, B) The inset graph of this figure shows linear range. Integration potential range for the admittance is 0 to 800 mV

The determination of OCA was done in optimal conditions. In this figure, each data point represents the measured sensor response for 3 consecutive additions injections of the OCA standard solutions. The inset graph of this figure shows the linear part of the calibration curve. The regression equation was  $\Delta Q$  (uC) = 0.1321x + 0.034(nM), with a correlation coefficient of  $R^2 = 0.993$ . The response time was about 6s. The estimated detection limit based on signal to noise ratio (S/N=3), was found  $3.7 \times 10^{-12}$  M. A determined unit of OCA-spiked real samples was analyzed with the help of the sensor. The results are shown in Table 1. The experimental results indicated a good recovery. These results showed that the proposed AuNPs/RGNS-MWCNT-IL/GCE biosensor can be applied successfully for the determination of OCA, by FFTCAV voltammetry.

**Table 1.** Recovery of OCA from certified reference

Added ( $\mu\text{g mL}^{-1}$ )	Found ( $\mu\text{g mL}^{-1}$ )	Recovery (%)
8.00	7.76	97.0
10.00	9.65	96.5
12.50	12.43	99.4
25.00	24.70	99.8
50.00	49.35	98.7
75.00	74.40	99.2
100.00	96.40	96.4

A long-term storage stability of the Au NPs/RGNS-MWCNT-IL/GCE was tested for 90 days, and it was seen that the sensitivity retained 97.8%, which gradually decreases afterwards might be due to the loss of the nanomaterial in from the surface. In evaluation, the performances of sensor is compared with some of the best previously reported OCA meth determination of odOCA, based on using different detection techniques (Table 2). and it was confirmed that the presented electrochemical method based on combination of a new OCA sensor with FFTCAV demonstrated an excellent and reproducible sensitivity [35-38].

**Table 2.** The comparison of the proposed sensor with the best previous reported ones based on the utilization of different materials

Ref.	Detection method	DL	Materials
[2735]	Immunosensor	0.01ng/mL	Functionalized magnetic nanoparticles
[2836]	Amperometry and Voltammetry	0.07 ng/mL	DNA biotinylated aptamer
[2937]	Voltammetry	0.25 ng/L	immobilization of azido-aptamer onto electrografted binary film via click

chemistry			
[3038]	FFT Cyclic Voltammetry	$2.2 \times 10^{-10}$ M	Au NPs /RGNSIL/GCE
This work	FFTCAV	$3.7 \times 10^{-12}$ M	Au NPs/RGNS-MWCNT-IL/GCE

#### 4. CONCLUSIONS

In this paper, an ultra-sensitive OCA measurement method was successively employed to elucidate the charge transfer changes occurring during the preparation and utilization of the sensor. The sensor been fabricated by modifying the GC electrode surface with Au NPs/RGNS-MWCNT-IL. A special electrochemical technique FFTCAV (which developed in our lab) was used to enhance the sensitivity of the measurement. The sensor exhibited good analytical characteristics, such as higher affinity of OCA towards Au NPs/RGNS-MWCNT-IL/GCE with a good repeatability and reproducibility. The sensor reported here is a good example of an the interaction between OCA and NPs on the GCE surface. A higher producible sensitivity, response time less than 6 s and detection limit of 3.7 pM was observed for the sensor. Nevertheless, this technique is a very effective tool for investigating probing the characteristics of a surface modified electrode.

#### ACKNOWLEDGEMENT

The authors are grateful to the Research Council of University of Tehran for the financial support of this work (under grant number 6102027/ 230-24580).

#### References

1. I. H. Ali and A. A. Ateeg, *Int. J. Environ. Res.*, 9 (2015) 291
2. S. M. Zhao, B. Wang, D. W. Wang, X. M. Li, B. Huang, P. Hu, L. W. Zhang and X. J. Pan, *Int. J. Environ. Res.*, 8 (2014) 317
3. T. Jeyakumar, I. Kalaiarasi, A. Rajavel, M. Anbu and R. kumar, *Int. J. Environ. Res.*, 8 (2014) 493
4. M. Manubolu, S. Eklund, P. C. Dutta and F. Malmlof, *Int. J. Environ. Res.*, 8 (2014) 733
5. F. Abdolahpur Monikh, M. Hosseini, J. Kazemzadeh Khoei and A. F. Ghasemi, *Int. J. Environ. Res.*, 8 (2014) 839
6. M. A. L. Milhome, P. L. R. Sousa, F. A. F. Lima and R. F. Nascimento, *Int. J. Environ. Res.*, 9 (2015) 255
7. S. Net, D. Dumoulin, R. El-Osmani, S. Rabodonirina and B. Ouddane, *Int. J. Environ. Res.*, 8 (2014) 1159
8. Bacaloni, C. Cavaliere, A. Faberi, E. Pastorini, R. Samperi, and A. Laganà, *J. Agric. Food Chem.*, 53 (2005) 5518.
9. T. Li, E.J. Jo and M.G. Kim, *Chem. Commun.* 48 (2012) 2304.
10. N. Adányi, I. A. Levkovets, S. Rodriguez-Gil, A. Ronald, M. Váradi and I. Szendrő, *Biosens. Bioelectron.*, 22 (2007) 797.
11. M. Benvenuto, J. Romano, and J.A. Krol, Unified method for mixed mycotoxin analysis using UV

- and fluorescence detection, *Waters Application Note* 2003, Waters Corporation.
12. Kearney G., and T. Bernsmann, A method for the rapid and sensitive determination of ochratoxin A in red wine, *Waters Application Note*, 2003, Waters Corporation.
  13. A.K. Geim, *Science*, 324 (2009) 1530.
  14. D.R. Dreyer, S.J. Park, C.W. Bielawski, R.S. Ruoff, *Chem. Soc. Rev.*, 39 (2009) 228.
  15. X. Huang, Z.Y. Yin, S.X. Wu, X.Y. Qi, Q.Y. He, Q.C. Zhang, Q. Y. Yan, F. Boey and H. Zhang, *Small*, 7 (2011) 1876.
  16. H. Zhang, and H. Cui, *Langmuir*, 25 (2009) 2604.
  17. M.N. Zhang, L. Su, and L.Q. Mao, *Carbon*, 44 (2006) 276.
  18. P. Norouzi, M. R. Ganjali, B. Larijani, A. Mirabi-Semnakolaii, F. S. Mirnaghi, and A. Mohammadi, *Pharmazie* 63 (2008) 633.
  19. T. Alizadeh, M. R. Ganjali, M. Zare, and P. Norouzi, *Electrochim. Acta* 55 (5), 1568-1574 (2010).
  20. P. Norouzi, M. R. Ganjali, S. Shirvani-Arani, and A. Mohammadi, *J. Pharm. Sci.* 95 (2007) 893.
  21. P. Norouzi, M. R. Ganjali, A. Sepehri, and M. Ghorbani, *Sens. Actuators B* 110 (2005) 239.
  22. P. Norouzi, M. R. Ganjali, M. Zare, and A. Mohammadi, *J. Pharm. Sci.* 96 (2007) 2009.
  23. P. Norouzi, M. R. Ganjali, and P. Matloobi, *Electrochem. Commun.* 7 (2005) 333.
  24. P. Norouzi, B. Larijani, M. Ezoddin and M. R. Ganjali, *Mater. Sci. Eng. C* 28 (2008) 87.
  25. P. Norouzi, B. Larijani, F. Faridbod and G. R. Ganjali, *Int. J. Environ. Res.*, 9 (2015) 101
  26. M. Sun, Z. Liu, K. Welsher, J.T. Robinson, A. Goodwin, S. Zaric et al. *Nano Res*, 1 (2008) 203.
  27. A. Wojcik, and P.V. Kamat, *ACS Nano*, 4 (2010) 6697.
  28. P. Norouzi, M. R. Ganjali, and L. Hajiaghababaei, *Anal. Lett.*, 39 (2006) 1941.
  29. P. Norouzi, G. R. Nabi Bidhendi, M.R. Ganjali, A. Sepehri, M. Ghorbani, *Microchim. Acta*, 152 (2005) 123.
  30. P. Norouzi, M. R. Ganjali, T. Alizadeh, and P. Daneshgar, *Electroanalysis*, 18 (2006) 947.
  31. M. R. Ganjali, P. Norouzi, R. Dinarvand, R. Farrokhi, and A. A. Moosavi-Movahedi, *Mater. Sci. Eng. C* 28 (2008) 1311.
  32. P. Norouzi, B. Larijani, F. Faridbod, M. R. Ganjali, *Int. J. Electrochem. Sci.*, 8 (2013) 6118.
  33. P. Norouzi, B. Larijani, M. R. Ganjali, and F. Faridbod, *Int. J. Electrochem. Sci.*, 9 (2014) 3130.
  34. P. Norouzi, B. Larijani, M. R. Ganjali, and F. Faridbod, *Int. J. Electrochem. Sci.*, 7 (2012) 10414.
  35. L. Zamfir, I. Geana, S. Bourigua, L. Rotariu, C. Bala, A. Errachid, and N. Jaffrezic-Renault, *Sens. Actuators B*, 159 (2011) 178.
  36. L. Bonel, J. C. Vidal, P. Duato, and J. R. Castillo, *Biosens. Bioelectron.*, 26 (2011) 3254.
  37. A. Hayata, A. Sassolasa, J. Martya, and A. Radib, *Talanta*, 103 (2013) 14.
  38. P. Norouzi, B. Larijani, and M. R. Ganjali, *Int. J. Electrochem Sci.* 7 (2012) 7313.